Influence of pH on Hydrothermal Synthesis of Photoactive Cu₂O Films in an Acetate Solution

Kexing Liu, Qiushi Song, Hongwei Xie, Zhiqiang Ning*

School of Metallurgy, Northeastern University, Shenyang 110819, China
*E-mail: songqs@smm.neu.edu.cn

Hydrothermal synthesis is an effective method to prepare p-type Cu₂O semiconductors as photocathode for electrochemical water splitting. Herein, Cu₂O films were prepared by hydrothermal synthesis in an acetate solution. The role of pH for the formation of Cu₂O during the synthesis was systemically investigated. The formation of Cu₂O was considered from thermodynamics. The relationship between the solution pH and the characteristics of the films, as well as the performance of the Cu₂O photocathode was established. The results showed that solution pH was an important factor for preparing uniform Cu₂O films. The stability region of Cu₂O shrunk with decreasing the concentration of Cu^{2+} ions in the acetate solution. The stability of Cu₂O was promoted by increasing the pH value. The homogeneity and the microstructure of Cu₂O films can be modified by optimizing the pH values.

Keywords: Cu₂O films; hydrothermal synthesis; pH value; Eh-pH diagram; photocathode

1. INTRODUCTION

Hydrogen energy is one of promising alternatives to relieve the serious problem of greenhouse gases derived from burning fossil energy [1]. The splitting of water based on solar energy is an attractive strategy to produce hydrogen gas owing to the abundance of water and sunlight. Photoelectrochemical (PEC) water splitting has drawn increasing attention in recent years because it integrates solar energy collection and water electrolysis into a single cell [2-7]. Various semiconductors such as perovskites, phosphides, metal-chalcogenides and metal oxides have been employed for electrode materials of the PEC cell [8, 9].

Metal oxides present attractive characteristics for solar-driven water splitting, such as widespread light harvesting, redox compatible energy levels, low cost and good stability [10, 11]. Cu₂O is extensively investigated as a photocathode material owing to its excellent properties of a narrow bandgap (~2 eV) [12-14], a high absorption coefficient (~10^5 cm⁻¹) and a theoretical photocurrent of -14.7

mA·cm^{-2} [5, 6, 15, 16]. These properties guarantee Cu_2O a suitable material to achieve high light-to-hydrogen conversion efficiency (~18 % under AM 1.5 illumination) [11, 17-21].

Several methods have been employed to synthesize photoactive Cu_2O films such as electrodeposition [2, 5], hydrothermal synthesis [3, 22, 23], thermal oxidation [24], anodic oxidation [25, 26] and magnetron sputtering [27, 28]. Hydrothermal synthesis has unique properties of easy operation, relatively low cost and simple apparatuses among these methods. To date, Cu_2O films were reported by hydrothermal synthesis and the reaction mechanism was also discussed [2, 3, 5, 23, 29]. In addition, the effect of some factors such as the type of anions, temperature, surfactants and the reaction time on the structure, morphology and PEC performance of Cu_2O films were also investigated. As a key point for the structural characteristics and PEC performance of Cu_2O films, the effect of pH on the prepared Cu_2O films was not comprehensively considered.

In this work, Cu_2O films were prepared by hydrothermal synthesis in a typical acetate solution. The influence of pH value on the formation of Cu_2O film was systemically discussed based on both thermodynamics and experimental results. The morphology and the crystalline structure of the Cu_2O films were characterized. The PEC performance of the Cu_2O films was investigated under simulated illumination.

2. EXPERIMENTAL

$Cu(CH_3COO)_2·H_2O$, NaOH and Polyvinylpyrrolidone (PVP, K-30) were purchased from Shanghai Aladdin Biochemical Technology Co., Ltd. Na_2SO_4 and NaOH were from Sigma-Aldrich Co. Ltd. All the chemicals were of analytical grade and used without further purification. Cu sheets were commercially available with a purity of 99.99 wt.%.

A Cu sheet (15×20×1mm) was firstly polished with sandpaper for a mirror-like surface. The sheet was ultrasonically washed with ethanol and deionized water to remove impurities on the surface and subsequently dried at room temperature. In a typical hydrothermal synthesis, $Cu(CH_3COO)_2·H_2O$ (0.667 g) was dissolved in 50 mL deionized water (the concentration of Cu^{2+} ions: 0.0667 mol·L^{-1}). Then 0.3 g of PVP was added into the solution with continuous stirring for 1 h. The pH value of the solution was adjusted with acetic acid and NaOH. The solution was transferred into a 100 mL stainless steel autoclave lined with Teflon. Subsequently, a Cu sheet was immersed into the solution. The autoclave was heated to 200 °C for 4 h and then was cooled down to room temperature. The sample was washed repeatedly with deionized water and dried for characterization. The pH value of the solution was adjusted to 3.4, 3.8, 5.6, 6.1, 6.2 and 6.3. Correspondingly, the samples prepared by hydrothermal synthesis was marked as A, B, C, D, E and F.
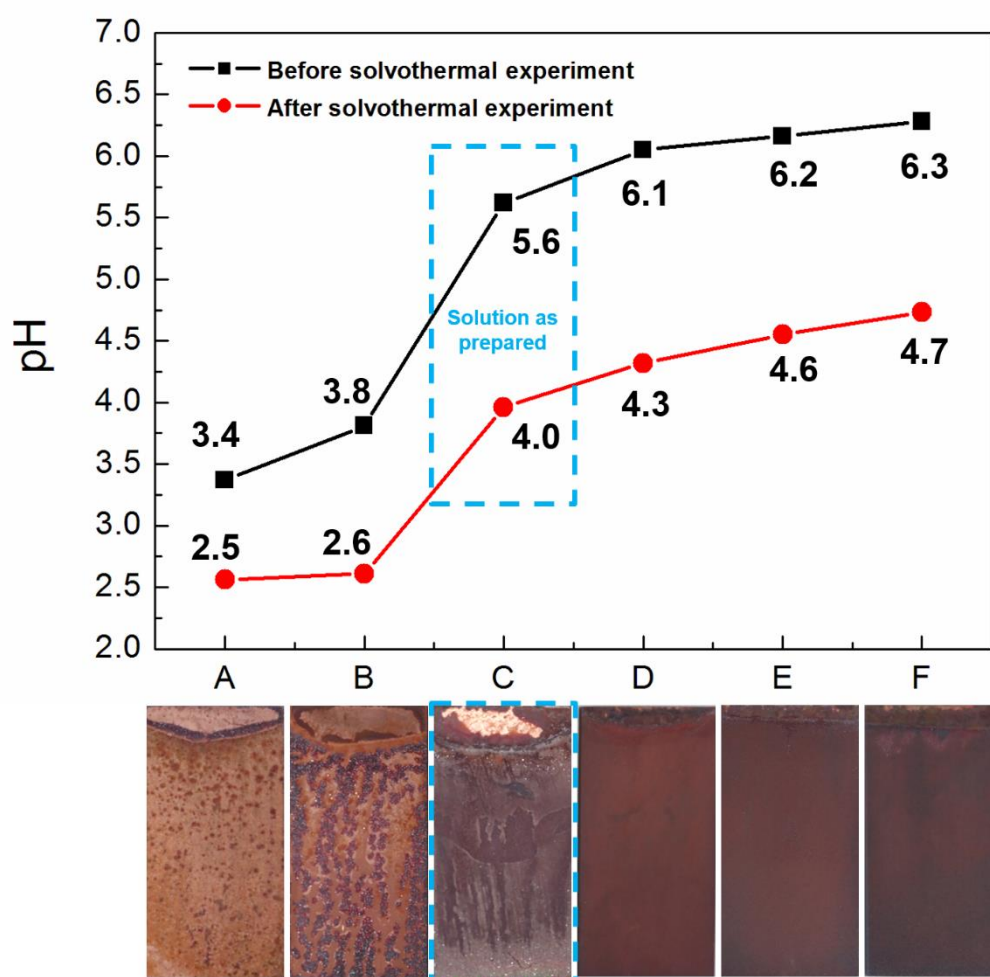
Phase composition of the samples was determined by a Shimadzu X-ray 6000 X-ray diffractometer equipped with Cu Kα1 radiation (XRD, λ = 1.5405 Å). Microstructure of the films were observed by a FEI Quanta FEG 250 scanning electron microscope (SEM). The UV-vis diffuse reflectance spectra were measured using a PerkinElmer Lambda 750s spectrophotometer.

PEC performance of the Cu_2O film was evaluated with a three-electrode configuration. The film, saturated Ag/AgCl and a Pt sheet (10×10×0.2mm) was used as the working electrode, the counter

electrode and the reference electrode, respectively. The PEC measurements were carried out in a 0.1 M sodium sulfate solution (pH = 5.8). Photoresponse of the samples was recorded by a 300 W xenon-arc lamp equipped with ultraviolet and infrared filters. AM 1.5 stimulated illumination (100 mW·cm^{-2}) was calibrated with a Si diode. Linear sweep voltammetry (LSV) was carried out by a CHI660E potentiostat with a scanning rate of 10 mV·s^{-1}. Photocurrent stability of the films was tested under chopped light irradiation (light/dark cycles of 20 s) at a fixed potential of 0 V versus RHE. The Mott-Schottky plots were measured at a fixed frequency of 1 kHz (sinusoidal perturbation: 5mV) with a linear scan from 0.3 to 0.9 V versus RHE.
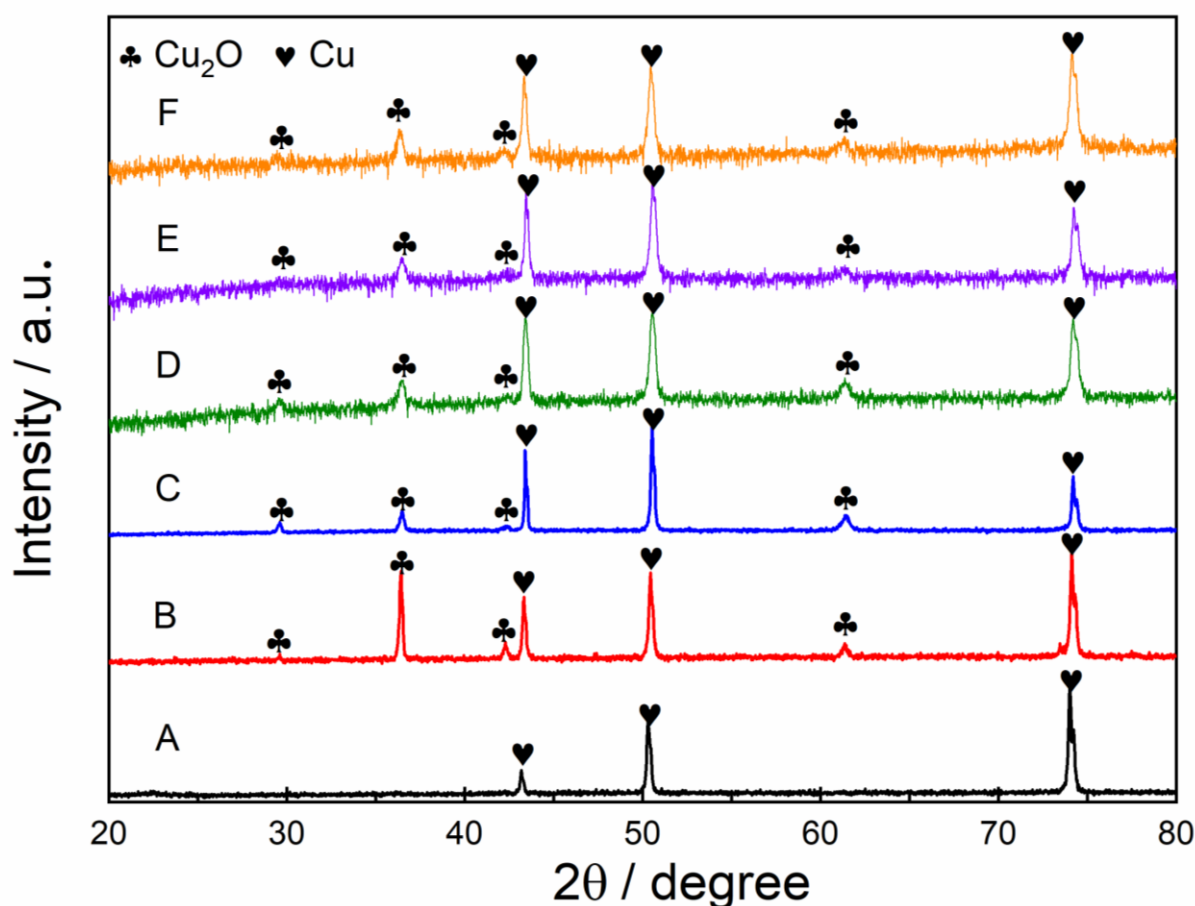
3. RESULTS AND DISCUSSION

The initial pH value of the as-prepared solution is 5.6. This value decreased to 4.0 after 4 h of hydrothermal synthesis at 200 °C, as highlighted in Figure 1 (the light blue dash line).

Figure 1. Variation of pH and digital photos of the samples prepared with different initial pH values in hydrothermal synthesis

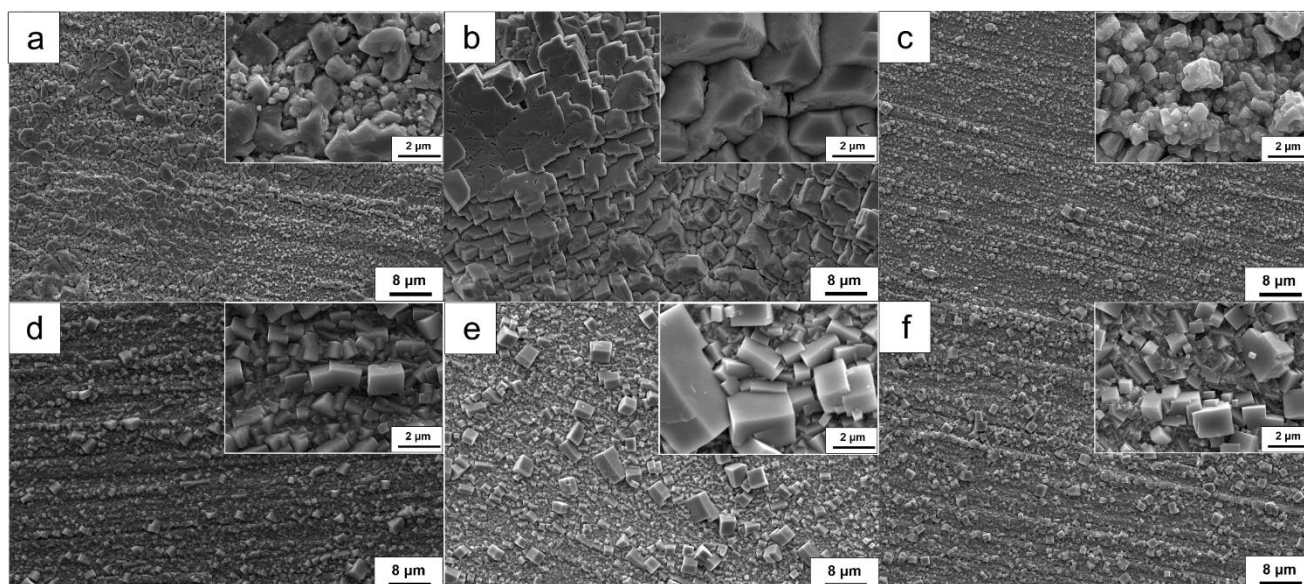*Int. J. Electrochem. Sci.,* 17 (**2022**) Article Number: 220660

4

The sample (Sample C) was not uniform with many coarse particles on the surface (the highlighted photograph in Figure 1). This sample is different from the Cu_2O films prepared in similar solutions [3, 22, 23, 30]. It was found that the initial pH values of the solution varied slightly in these studies. Therefore, it can be predicted that the solution pH plays an important role for hydrothermal synthesis of Cu_2O films. The final pH values of the solution were also plotted in Figure 1. Brick red deposit was prepared on the Cu plate when the pH varied between 2.5 and 3.4 (Sample A). Some dark red scales appeared on the surface in the pH range of 2.6-3.8 (Sample B). The Cu sheet was almost covered by scarlet deposit with the co-existence of some coarse crystals in the as-prepared solution (4.0-5.6, Sample C). The dark red deposit was an indicator for the formation of Cu_2O [23]. Afterward, the deposit presented a uniform dark red surface once the initial pH values were higher than 5.6 (Samples D-F).

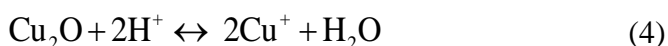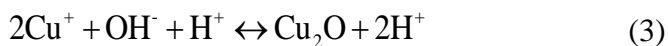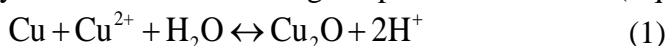**Figure 2.** XRD patterns of the samples prepared in different pH regions (Samples A-F)

Figure 2 shows the XRD patterns of Samples A-F. The diffraction peaks of Cu_2O were not indexed at a relatively lower pH value (Sample A). A Cu_2O phase gradually appeared once the solution pH was adjusted to higher values (Samples B-F). The diffraction peaks of Cu_2O increased intensively due to the thick oxide scales on Sample B. Figures 3a-3f present the SEM images of Samples A-F,

respectively. Granular particles can be observed on Sample A (Figure 3a). The particles were not uniform according to the magnified SEM image (the inset in Figure 3a). The red scales on Sample B consisted of many bulk particles (Figure 3b). The particles were obviously bigger than the granular ones on Sample A. The Cu_2O particles were more uniform on Sample C (Figure 3c), but most of them had irregular edges. The deposit prepared on the Sample D (Figure 3d) mainly consisted of cubic particles (Figure 3d). These particles are close to the well-developed Cu crystals in the literature [2, 4]. The cubic particles tended to be inhomogeneous with further enhancing the solution pH (Figures 3e-3f). In summary, the homogeneity and microstructure of the Cu_2O films prepared by hydrothermal synthesis varied with the pH region of the solution.
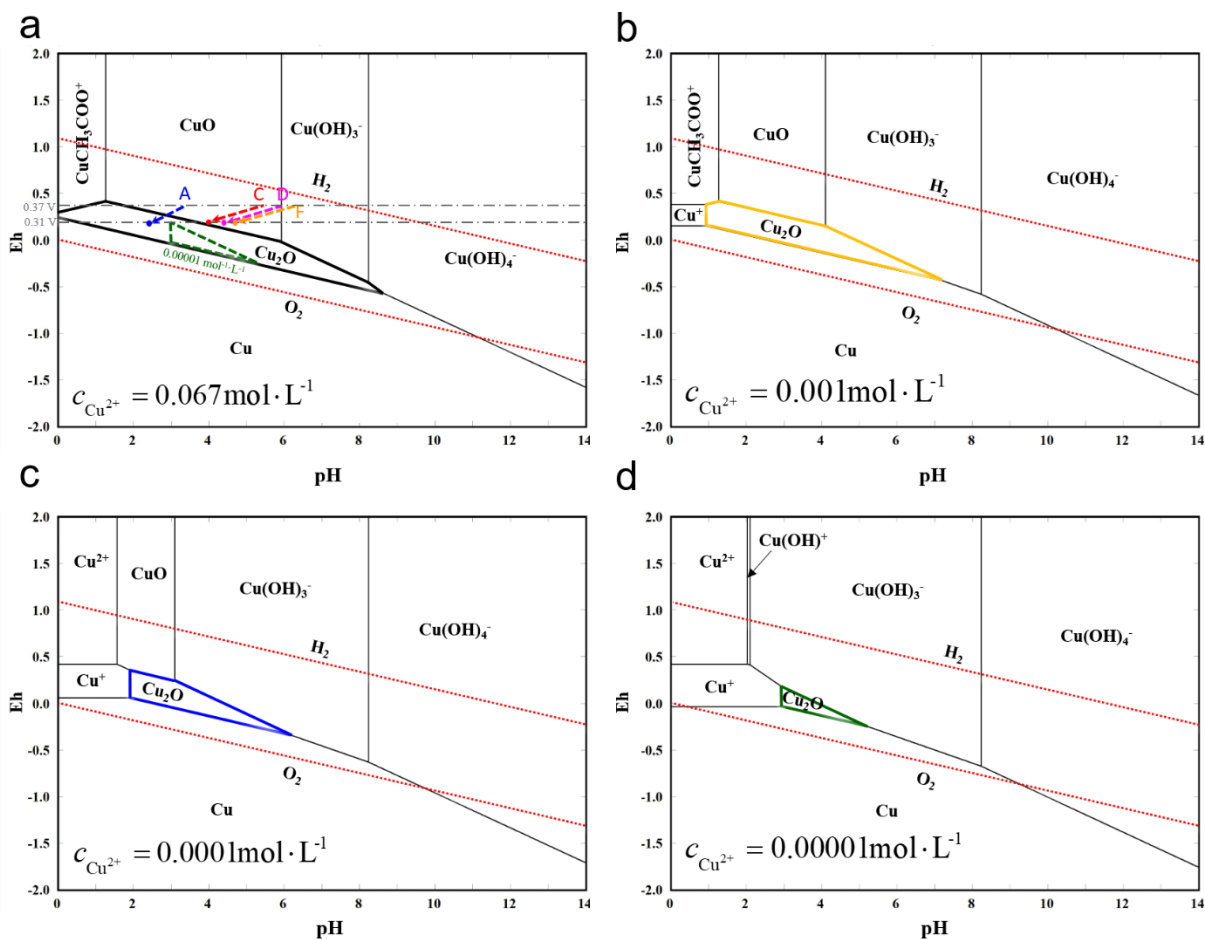

Figure 3. SEM images of the Samples prepared in different pH regions (Samples A-F)

The influence of pH on the formation of Cu_2O was considered from thermodynamics because the stability and activity of Cu_2O changed with the solution pH. Cu_2O is formed by a disproportionation reaction between Cu^{2+} ions and Cu substrate (Eq. 1) in the synthesis [22]. It can also be generated by Eqs. 2-3, in which the Cu^+ ion is a vital and indispensable intermediate [22]. The formation of Cu_2O is ascribed to the saturation of Cu^+ ions due to its limited solubility [22].Then the solution pH decreased with proceeding the hydrothermal synthesis because of continuous consumption of OH^+ ions. This conclusion agrees with the variation of solution pH in Figure 1. Therefore, the previously formed Cu_2O possibly dissolved as decreasing the pH in the solution (Eq. 4) [22].

$$Cu + Cu^{2+} + H_2O \leftrightarrow Cu_2O + 2H^+ \qquad (1)$$

$$Cu + Cu^{2+} \leftrightarrow 2Cu^+ \qquad (2)$$

$$2Cu^+ + OH^- + H^+ \leftrightarrow Cu_2O + 2H^+ \qquad (3)$$

$$Cu_2O + 2H^+ \leftrightarrow 2Cu^+ + H_2O \qquad (4)$$

Pourbaix diagrams of Cu-H_2O-acetate systems were constructed to evaluate the stability of Cu_2O in the hydrothermal synthesis. The reactions involved in aqueous solutions can be generally expressed
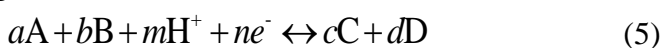
by Eq. 5 [31, 32]. The standard Gibbs free energy (ΔG^{θ}) for the equation is proportional to the standard electrode potential (E^{θ}) according to the Nernst equation (Eq. 6), in which n is the number of transferred electrons and F is Faraday's constant (96485 C·mol^{-1}). Therefore, the electrode potential (E_h) of this reaction is a function of time (t), temperature (T) and activities of the chemical species ($a_X^{v_i}$, $X = A, B, H^+, C, D$ and H_2O, $v_i = a, b, m, c, d$), as demonstrated in Eq. 7. R represents gas constant (96485 J·mol^{-1}·K^{-1}). The species selected to construct the Eh-pH diagrams were Cu^{2+}, Cu^+, Cu, CuO, Cu_2O, $Cu(OH)_3^-$, $Cu(OH)_4^{2-}$ and $Cu(CH_3COO^-)$. These species are all considered previously to build the Cu-H$_2$O-acetate diagrams [32, 33]. Thermodynamic data of these species are available in the literature [32, 34-37]. The ΔG^{θ} for all reactions considered in this work was listed in Table 1. The concentrations of Cu^{2+} ions ($c_{Cu^{2+}}$) were fixed at 0.067, 0.001, 0.0001 and 0.00001 mol^{-1}·L^{-1}. The temperature was 200 °C and the total pressure was estimated at 1.53 MPa.

Figure 4. Eh-pH diagram of Cu-H$_2$O–Acetate system at 473 K with (a) 0.067; (b) 0.001; (c) 0.0001 and (d) 0.00001 mol·L^{-1} Cu^{2+} ions

Figures 4a-4d shows the Cu-H$_2$O-acetate pourbaix diagrams developed in this work. It was found that the stability region of Cu$_2$O shrunk with decreasing the concentration of Cu^{2+} ions. Meanwhile, the stability region of Cu$^+$ ions gradually expanded. The concentration of Cu^{2+} ions was less than 1 wt.%,

so the activities of copper species can be represented by their concentrations. The initial potential of the Cu^{2+}/Cu redox couple was estimated at 0.37 V once a Cu plate was immersed in the $Cu(CH_3COO)_2$ solution ($c_{Cu^{2+}}$ = 0.067 mol·L^{-1}). The potential decreased to 0.31 V when $c_{Cu^{2+}}$ reached 0.00001 mol·L^{-1}. Therefore, the pH regions of the solution are important for the formation of Cu_2O. Taking sample C as an example, the solution pH varied from 5.6 to 4.0 during 4 h of hydrothermal synthesis. Then the coordinate of the terminal point is (4.0, 0.31) in the Eh-pH diagram (red point in Figure 4a). The terminal points of Samples A, D and F were also marked in the diagram (blue, purple and yellow points). It was found that the terminal points or their extension lines tended to contact the stability region of Cu_2O more favorably with increasing the initial pH of the solution. The terminal point deviated from the stability region of Cu_2O in an acidic environment, e.g. Sample A. Therefore, the formation of a Cu_2O layer was not favorable in thermodynamics. The Eh-pH diagrams present equilibrium states in the Cu-H_2O-acetate system, which may differ from the nonequilibrium states of the species in the autoclave. However, the relative location of the solution pH and the stability region of Cu_2O also reveals the role of pH for forming Cu_2O.
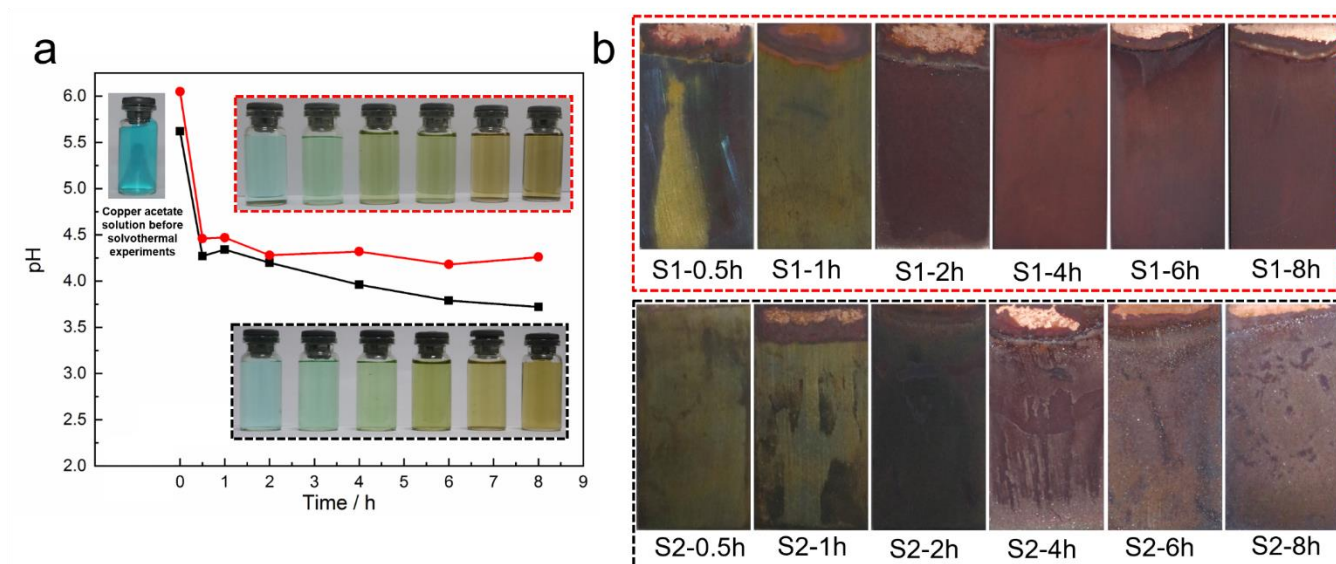
$$aA + bB + mH^+ + ne^- \leftrightarrow cC + dD \qquad (5)$$

$$\Delta G^\theta = -nFE^\theta \qquad (6)$$
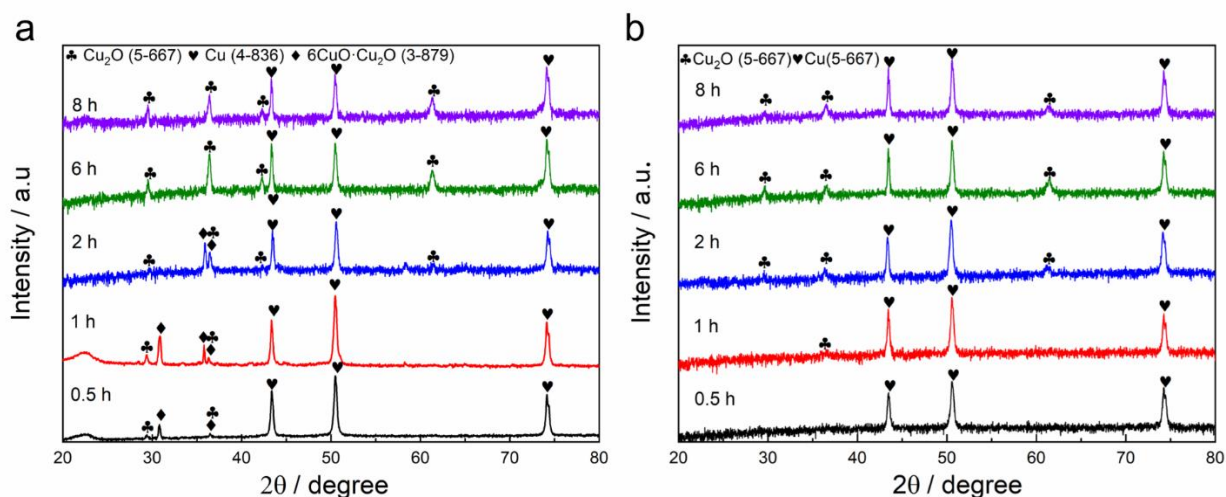
$$E_h = E^\theta - \frac{2.303RT}{nF} \log(\frac{a_C^c \cdot a_D^d}{a_A^a \cdot a_B^b}) - \frac{2.303RT}{F} \frac{m}{n} \cdot pH \qquad (7)$$

Two initial pH values (5.6 and 6.1) were selected to investigate the formation of Cu_2O films. The hydrothermal experiments were terminated for various durations. The solutions were defined as "S1" and "S2". The samples were named as Sx-yh (x =1 or 2, y refers duration). Figure 5a shows the variation of pH values during the synthesis as well as digital photos of the solutions. In general, the solution pH dropped sharply at the beginning and then maintained at a relatively value. The final pH is relatively higher in S2. The color of the solutions faded with extending the duration, indicating continuous consumption of Cu^{2+} ions. Though the color of S1 did not show obvious difference from that of S2, the samples obtained in S1 and S1 had different optical appearance, as shown in Figure 4b. The S1-0.5h had a yellow-green surface (the lower part in Figure 4b). Several black regions appeared on the surface of S1-1h. The surface changed to black after 2 h of synthesis (S1-2h). Though brick red samples were obtained with further extending the durations (S1-4h, S1-6h and S1-8h), the films were not homogeneous with many bigger particles on the surface. On the contrary, the black regions were not observed once the hydrothermal synthesis was carried out in S2 (the upper part in Figure 4b). The surface color was yellow-green at the beginning (S2-0.5h and S2-1h) and turned to brick red promptly when the duration was longer than 2 h (S2-2h, S2-4h, S2-6h and S2-8h). In addition, the deposits are uniform across Cu substrates.

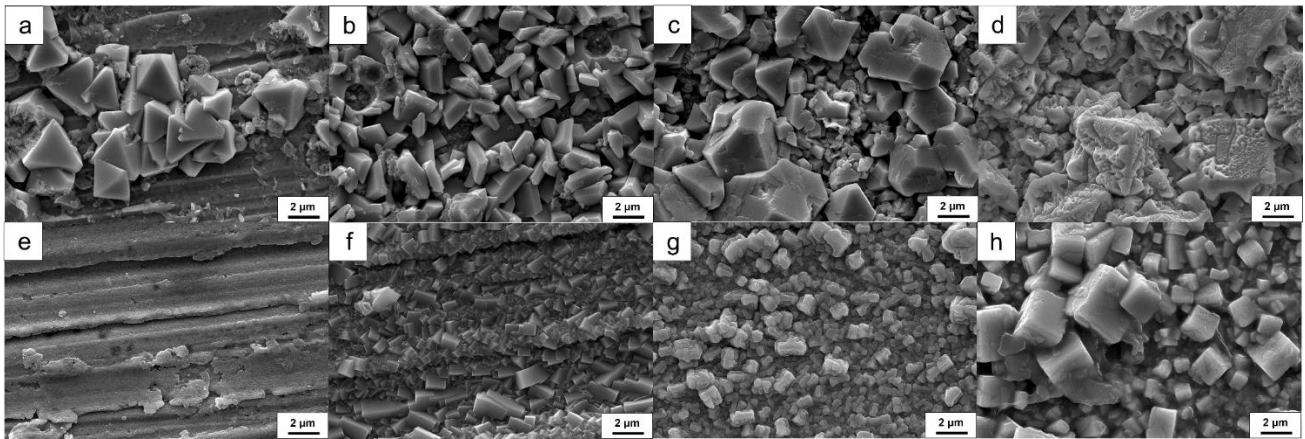*Int. J. Electrochem. Sci.*, 17 **(2022)** Article Number: 220660

8

Figure 5. (a) Variation of pH value and digital photos of solutions; (b) digital photos of the samples synthesized for various durations in S1 and S2
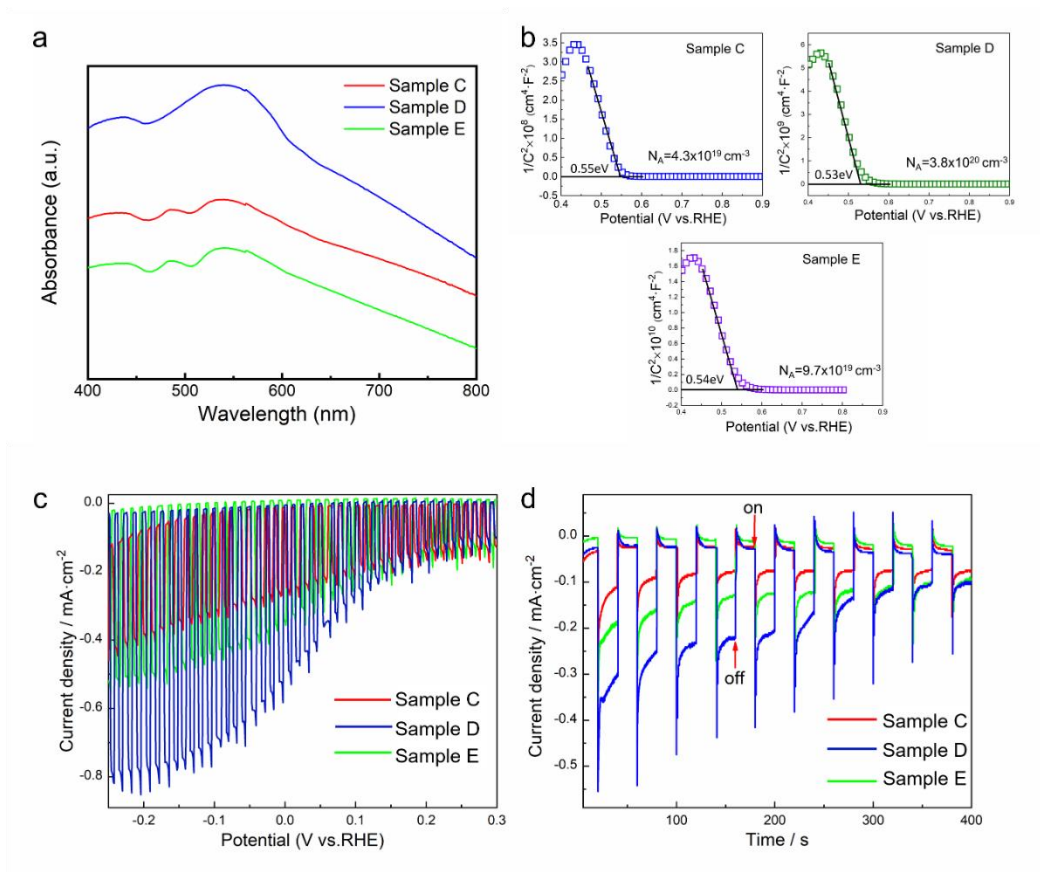

Figure 6. XRD patterns of the samples for various durations in (a) S1 and (b) S2

XRD analysis was performed to determine the phases appeared during the synthesis in S1 and S2. A Cu_4O_3 (paramelaconite) phase was documented for the samples prepared in S1 (Figure 6a). This phenomenon indicates that CuO was formed in the synthesis since Cu_4O_3 can be generated from CuO and Cu_2O at elevated temperatures [29, 38]. Cu_4O_3 was also transformed to Cu_2O with proceeding the synthesis. However, the diffraction peaks of CuO or Cu_4O_3 were not found when hydrothermal synthesis was carried out in S2 (Figure 6b). It implies that CuO was not a stable phase when the pH varied between 4.3 and 6.1. This result agrees well with the stability of CuO and Cu2O from the Eh-pH diagrams. The terminal point of solution pH may located in the stable region of CuO if the solution pH was at a relatively lower value (Figures 4a).

Figure 7. SEM images of (a) S1-0.5h; (b) S1-2h; (c) S1-6h; (d) S1-8h; (e) S2-0.5h; (f) S2-2h; (g) S2-6h; (h) S2-8h

Figure 8. (a) UV-vis absorption spectra; (b) Mott-Schottky plots of Samples C, D and E; (c) Linear sweep voltammograms; (d) Chronoamperometric stability measurement of Samples C, D and E biased at 0 V vs RHE in a 0.5 M sodium sulfate electrolyte (pH=5.8) under chopped light illumination

Figures 7a-7d shows SEM images of the samples prepared in S1. Several octahedral particles aggregated on S1-0.5h (Figure 7a). The shape of the deposited particles became irregular and the number increased significantly with extending the duration (Figures 2c and 7b-7d). On the contrary, a thin film

was synthesized on S2-0.5h (Figure 7e). The particles involved in the film were obviously smaller than the aggregated octahedral particles on S1-0.5h. The particles evolved to cubic grains after 2 and 4 h of synthesis (Figure 2d and Figure 7e). However, the cubic crystals were destroyed in a long-duration synthesis (Figures 7g-7h). The concentration of H^+ increased with proceeding the hydrothermal synthesis. This lead to the erosion of the previously formed Cu_2O crystals (Eq. 4). Therefore, the pH values alter not only the stability of the products, but also the nucleation and growth of the Cu_2O films. The control of solution pH is a key factor to prepare Cu_2O films in an acetate solution.

The Cu_2O films were preliminarily evaluated as the photocathode for electrochemical splitting of water. The UV/Vis diffuse reflectance spectra of the Cu_2O films prepared at different pH values were compared in Figure 8a. The absorption intensity of Sample D is higher than that of Samples C and E. It reveals that Sample D has greater light-absorption ability than Samples C and E [3]. The outstanding photoabsorption property of Sample D is attributed to the better developed Cu_2O crystals in the film. Figure 8b shows the Mott-Schottky plots of Samples C, D and E. All the plots exhibit a negative slop, which is an indicator of a p-type semiconductor [39, 40]. The flat band potentials (V_{FB}) of Sample C, D and E were estimated at 0.55, 0.53 and 0.54 V vs. RHE, respectively. Meanwhile, the calculated carrier densities were 4.3×10^{19}, 3.8×10^{20} and 9.7×10^{19} cm^{-3}. These results indicate that pH values of the solution have little influence on the flat band potential [39, 41]. However, the carrier density was enhanced by positively shifting the solution pH. The reason for this enhancement is attributed to well development of the Cu_2O grains and the decrease of surface defects on the grains [42]. Sample C exhibits the highest carrier density among the samples. Photocurrent response of the Cu_2O films was measured under periodically chopped illumination. Figure 8c presents typical linear sweep voltammetry (LSV) of Samples C, D and E in a negative potential scan. The photocurrent density of Sample C reached about -0.6 $mA \cdot cm^{-2}$. This value is comparable to the result in literature [22, 24]. Sample C presents the highest photocurrent density during the chronoamperometric stability measurement biased at 0 V vs. RHE. The superior PEC performance of Sample C over Sample D and E is mainly attributed to the difference of characteristics of the films, such as crystallinity, morphology and homogeneity [42]. The characteristics can be effectively modified by adjusting the solution pH in the hydrothermal synthesis.

4. CONCLUSIONS

Homogeneous Cu_2O films consisted of cubic grains were successfully prepared by hydrothermal synthesis in an acetate solution. The pH value of the acetate solution was a key factor to synthesize Cu_2O films. The morphology, phase composition and homogeneity of the films can be modified by adjusting the solution pH. The influence of the solution pH was explained with Cu-H_2O-acetate E_h-pH diagrams. The stability region of Cu_2O shrunk with proceeding the hydrothermal synthesis. It caused the mismatch of the E_h/pH value of the solution and the stability region of Cu_2O. Consequently, other Cu-involved species such as Cu_2O and Cu_4O_3 were formed in the deposits. The undesirable consequence can be prevented by adjusting the solution pH. Cupric oxides disappeared when the pH region was higher than 6.1-4.3. The PEC performance is associated with the characteristics of the films, which can also be optimized by adjusting pH values of the acetate solution.

References

1. X. Hao, Y. Hu, Z. Cui, J. Zhou, Y. Wang and Z. Zou, *Appl. Catal. B*, 244 (2019) 694.
2. Y. C. Chen, Z. Q. Hsiao and Y. K. Hsu, *Int. J. Hydrog. Energy*, 43 (2018) 13032.
3. R. Ji, W. Sun and Y. Chu, *Chemphyschem*, 14 (2013) 3971.
4. A. Paracchino, V. Laporte, K. Sivula, M. Graetzel and E. Thimsen, *Nat. Mater.*, 10 (2011) 456.
5. Y.C. Chen, Y.J. Chen, P.H. Dong and Y.K. Hsu, *ACS. Appl. Energy Mater.*, 3 (2020) 1373.
6. C.L. Li, T. Hisatomi, O. Watanabe, M. Nakabayashi, N. Shibata, K. Domen and J.J Delaunay, *Energy Environ. Sci.*, 8 (2015) 1493.
7. X. Yao, X. Zhao, J. Hu, H. Xie, D. Wang, X. Cao, Z. Zhang, Y. Huang, Z. Chen and T. Sritharan, *Iscience*, 19 (2019) 976.
8. M. Zhang, J. Wang, H. Xue, J. Zhang, S. Peng, X. Han, Y. Deng and W. Hu, *Angew. Chem. Int. Edit.*, 59 (2020) 18463.
9. C.Y. Toe, J. Scott, R. Amal and Y.H. Ng, *J. Photoch. Photobio. C*, 40 (2019) 191.
10. Y. Yang, S. Niu, D. Han, T. Liu, G. Wang and Y. Li, *Adv. Energy Mater.*, 7 (2017) 1700555.
11. Q. Huang, Z. Ye and X. Xiao, *J. Mater. Chem. A*, 3 (2015) 15824.
12. Y. Kwon, A. Soon, H. Han and H. Lee, *J. Mater. Chem. A*, 3 (2015) 156.
13. X. Chen, R. Chen, X. Zhu, Q. Liao, Y. Zhang, D. Ye, B. Zhang, Y. Yu and J. Li, *J. Catal.*, 372 (2019) 182.
14. D. Chen, Z. Liu, Z. Guo, W. Yan and M. Ruan, *Chem. Eng. J.*, 381 (2020) 122655.
15. Z. Jin, Z. Hu, J. C. Yu and J. Wang, *J. Mater. Chem. A*, 4 (2016) 13736.
16. A. Paracchino, N. Mathews, T. Hisatomi, M. Stefik, S.D. Tilley and M. Graetzel, *Energy Environ. Sci.*, 5 (2012) 8673.
17. I.V. Bagal, N.R. Chodankar, M.A. Hassan, A. Waseem, M.A. Johar, D.H. Kim and S.W. Ryu, *Int. J. Hydro. Energy*, 44 (2019) 21351.
18. J. Luo, L. Steier, M.K. Son, M. Schreier, M.T. Mayer and M. Graetzel, *Nano Lett.*, 16 (2016) 1848.
19. Z. Zhang and P. Wang, *J. Mater. Chem.*, 22 (2012) 2456.
20. A. Dubale, W.N. Su, A. Tamirat, C.J. Pan, B. Aragaw, H.M. Chen, C.H. Chen and B.J. Hwang, *J. Mate. Chem. A*, 2 (2014) 18383.
21. Y. Li, X. Zhang, H. Chen and Y. Li, *Catal. Commun.*, 66 (2015) 1.
22. L. Xiong, S. Huang, X. Yang, M. Qiu, Z. Chen and Y. Yu, *Electrochim. Acta*, 56 (2011) 2735.
23. D. Ursu, N. Miclau and M. Miclau, *Electron. Mater. Lett.*, 14 (2018) 405.
24. D.S. Zimbovskii and A.N. Baranov, *Mater. Sci. Eng.*, 525 (2019) 012018.
25. D.S. Zimbovskii and B.R. Churagulov, *Inorg. Mater.*, 54 (2018) 660.
26. G.N. Shelovanova and T.N. Patrusheva, *Phys. Solid State*, 59 (2017) 246.
27. D. Kudryashov, A. Monastyrenko, A. Mozharov, A. Bukatin, E. Nikitina, E. Pirogov and A.Gudovskikh, *J. Phys.: Conf. Ser.*, 917 (2017) 032020.
28. J. Gan, S. Gorantla, H.N. Riise, O.S. Fjellvag, S. Diplas, O.M. Lovvik, B.G. Svensson, E.V. Monakhov and A.E. Gunnaes, *Appl. Phys. Lett.*, 108 (2016) 152110 .
29. L. Zhao, H. Chen, Y. Wang, H. Che, P. Gunawan, Z. Zhong, H. Li and F. Su, *Chem. Mater.*, 24 (2012) 1136.
30. L. Pan, J.J. Zou, T. Zhang, S. Wang, Z. Li, L. Wang and X. Zhang, *J. Phys. Chem. C*, 118 (2014) 16335.
31. M. Pourbaix, *J. Electroanal. Chem.*, 13 (1967) 471.
32. K.M. Deen, N. Mehrjoo and E. Asselin, *J. Electroanal. Chem.*, 895 (2021) 115467.
33. B. Beverskog and I. Puigdomenech, *J. Electrochem. Soc.*, 144 (1997) 3476.

34. J.S. Seewald and W.E. Seyfried, *Geochim. Cosmochim. Acta*, 55 (1991) 659.
35. E. L. Shock, D. C. Sassani, M. Willis and D. A. Sverjensky, Geochim. Cosmochim. Acta, 61 (1997) 907.
36. E. L. Shock and C. M. Koretsky, Geochim. Cosmochim. Acta, 57 (1993) 4899.
37. P.A. Brook, *Corros. Sci.*, 12 (1972) 297.
38. L. Debbichi, M.C. Marco de Lucas and P. Krueger, *Mater. Chem. Phys.*, 148 (2014) 293.
39. W. Shi, X. Zhang, S. Li, B. Zhang, M. Wang and Y. Shen, *Appl. Surf. Sci.*, 358 (2015) 404.
40. S. John and S.C. Roy, *Appl. Surf. Sci.*, 509 (2020) 144703.
41. X. An, K. Li and J. Tang, *Chemsuschem*, 7 (2014) 1086.
42. S.K. Baek, J.S. Kim, Y.B. Kim, J.H. Yoon, H.B.R. Lee and H. K. Cho, *ACS Sustainable Chem. Eng.*, 5 (2017) 8213.